International Journal of Solids and Structures 50 (2013) 1930–1943

Contents lists available at SciVerse ScienceDirect

International Journal of Solids and Structures

journal homepage: www.elsevier.com/locate/ijsolstr

A sampling surfaces method and its application to three-dimensional exact solutions for piezoelectric laminated shells

G.M. Kulikov *, S.V. Plotnikova

Department of Applied Mathematics and Mechanics, Tambov State Technical University, Sovetskaya Street, 106, Tambov 392000, Russia

ARTICLE INFO

Article history:
Received 24 November 2012
Received in revised form 9 February 2013
Available online 22 February 2013

Keywords:
Piezoelectric laminated shell
Sampling surfaces method
3D exact solutions
Cross-ply shell
Angle-ply shell

ABSTRACT

The application of the sampling surfaces (SaS) method to piezoelectric laminated composite plates is presented in a companion paper (Kulikov, G.M., Plotnikova, S.V., Three-dimensional exact analysis of piezoelectric laminated plates via sampling surfaces method. International Journal of Solids and Structures 50, http://dx.doi.org/10.1016/j.ijsolstr.2013.02.015). In this paper, we extend the SaS method to shells to solve the static problems of three-dimensional (3D) electroelasticity for cylindrical and spherical piezoelectric laminated shells. For this purpose, we introduce inside the nth layer I_n not equally spaced SaS parallel to the middle surface of the shell and choose displacements of these surfaces as basic kinematic variables. Such choice of displacements permits, first, the presentation of governing equations of the proposed piezoelectric shell formulation in a very compact form and, second, gives an opportunity to utilize the strain–displacement equations, which precisely represent all rigid-body shell motions in any convected curvilinear coordinate system. It is shown that the developed piezoelectric shell formulation can be applied efficiently to finding of 3D exact solutions for piezoelectric cross-ply and angle-ply shells with a specified accuracy using a sufficient number of SaS, which are located at Chebyshev polynomial nodes and layer interfaces as well.

1. Introduction

In recent years, a considerable work has been carried out on the three-dimensional (3D) exact analysis of piezoelectric laminated shells. In the literature, there are at least four approaches to 3D exact solutions of electroelasticity for piezoelectric shells (see, e.g. survey papers of Tauchert et al., 2000; Wu et al., 2008); namely, the Pagano approach, the state space approach, the series expansion approach and the asymptotic approach. The first approach (Vlasov, 1957; Pagano, 1969, 1970) was recently implemented for a piezoelectric shell (Wu and Huang, 2009; Wu and Tsai, 2012), which is artificially divided into a large number of individual layers with equal thicknesses following an idea of Soldatos and Hadjigeorgiou (1990). The state space approach was utilized by Xu and Noor (1996), Chen et al. (2001), Wang and Zhong (2003) and Wu and Liu (2007). The most popular series expansion approach was extensively used by Chen and Shen (1996), Chen et al. (1996), Dube et al. (1996), Dumir et al. (1997), Heyliger (1997), Kapuria et al. (1997a,b) and Kapuria et al. (1997c,d). The 3D exact solutions based on the asymptotic shell formulation were obtained in contributions of Cheng and Reddy (2002), Wu et al. (2005), Wu and Syu (2007) and Wu et al. (2007).

The present paper is intended to show that the sampling surfaces (SaS) method can be also applied efficiently to 3D exact solutions of electroelasticity for piezoelectric cylindrical and spherical shells. In accordance with this method, we choose inside the nth layer I_n not equally spaced SaS $\Omega^{(n)1}, \Omega^{(n)2}, \ldots, \Omega^{(n)I_n}$ parallel to the middle surface of the shell and introduce the displacement vectors $\mathbf{u}^{(n)1}, \mathbf{u}^{(n)2}, \ldots, \mathbf{u}^{(n)I_n}$ of these surfaces as basic shell variables, where $I_n \geqslant 3$. Such choice of displacements permits, first, the presentation of governing equations of the proposed piezoelectric shell formulation in a very compact form and, second, gives an opportunity to utilize the strain–displacement equations, which precisely represent all rigid-body shell motions in any convected curvilinear coordinate system (Kulikov and Plotnikova, 2013a). The SaS method has been already utilized for the analysis of elastic plates and shells (Kulikov and Plotnikova, 2011b, 2012a,b) and piezoelectric plates (Kulikov and Plotnikova, 2013b). It is necessary to note that the term SaS should not be confused with such terms as fictitious interfaces or virtual interfaces, which are extensively used in layer-wise theories. The main difference consists in the lack of possibility to employ the polynomials of high degree in the thickness direction because in conventional layer-wise theories only the third and fourth order polynomial interpolations are admissible (see, e.g. Carrera, 2002, 2003; Carrera et al., 2011). This restricts the use of the fictitious/virtual interfaces technique for finding of 3D exact solutions of piezoelectricity. On the contrary, the SaS method

* Corresponding author. Tel.: +7 475 271 3299; fax: +7 075 271 0216.
E-mail addresses: kulikov@apmath.tstu.ru, gmkulikov@mail.ru (G.M. Kulikov).

0020-7683/$ - see front matter © 2013 Elsevier Ltd. All rights reserved.
http://dx.doi.org/10.1016/j.ijsolstr.2013.02.010

permits the use of polynomials of high degree. The latter gives an opportunity to derive the 3D exact solutions for piezoelectric laminated shells with a prescribed accuracy employing a sufficient number of not equally spaced SaS.

It should be mentioned that the developed approach with equally spaced SaS (Kulikov and Plotnikova, 2011b) does not work properly with Lagrange polynomials of high degree because the Runge's phenomenon can occur, which yields the wild oscillation at the edges of the interval when the user deals with any specific functions. If the number of equally spaced nodes is increased then the oscillations become even larger. Fortunately, the use of Chebyshev polynomial nodes (Burden and Faires, 2010) can help to improve significantly the behavior of Lagrange polynomials of high degree for which the error will go to zero as $I_n \to \infty$.

The authors restrict themselves to finding *five right digits* in all examples presented. The better accuracy is possible of course but requires more SaS inside each layer to be taken.

2. Kinematic description of undeformed laminated shell

Consider a thick laminated shell of the thickness h. Let the middle surface Ω be described by orthogonal curvilinear coordinates θ_1 and θ_2, which are referred to the lines of principal curvatures of its surface. The coordinate θ_3 is oriented along the unit vector $\boldsymbol{a}_3 = \mathbf{e}_3$ normal to the middle surface. Introduce the following notations: $\mathbf{r} = \mathbf{r}(\theta_1, \theta_2)$ is the position vector of any point of the middle surface; $\boldsymbol{a}_\alpha$ are the base vectors of the middle surface given by

$$\boldsymbol{a}_\alpha = \mathbf{r}_{,\alpha} = A_\alpha \mathbf{e}_\alpha, \tag{1}$$

where $\mathbf{e}_\alpha$ are the orthonormal base vectors and A_α are the coefficients of the first fundamental form; $\theta_3^{(n)i_n}$ are the transverse coordinates of SaS of the nth layer expressed as

$$\theta_3^{(n)1} = \theta_3^{[n-1]}, \quad \theta_3^{(n)I_n} = \theta_3^{[n]},$$

$$\theta_3^{(n)m_n} = \frac{1}{2}(\theta_3^{[n-1]} + \theta_3^{[n]}) - \frac{1}{2}h_n \cos\left(\pi \frac{2m_n - 3}{2(I_n - 2)}\right), \tag{2}$$

where $\theta_3^{[n-1]}$ and $\theta_3^{[n]}$ are the transverse coordinates of layer interfaces $\Omega^{[n-1]}$ and $\Omega^{[n]}$, and $h_n = \theta_3^{[n]} - \theta_3^{[n-1]}$ is the thickness of the nth layer; $\mathbf{R} = \mathbf{r} + \theta_3 \mathbf{e}_3$ is the position vector of any point in the shell body; $\mathbf{R}^{(n)i_n} = \mathbf{r} + \theta_3^{(n)i_n}\mathbf{e}_3$ are the position vectors of SaS of the nth layer; $\mathbf{g}_i$ are the base vectors in the shell body defined as

$$\mathbf{g}_\alpha = \mathbf{R}_{,\alpha} = A_\alpha c_\alpha \mathbf{e}_\alpha, \quad \mathbf{g}_3 = \mathbf{R}_{,3} = \mathbf{e}_3, \tag{3}$$

where $c_\alpha = 1 + k_\alpha \theta_3$ are the components of the shifter tensor and k_α are the principal curvatures of the middle surface; $\mathbf{g}_i^{(n)i_n}$ are the base vectors of SaS of the nth layer (see Fig. 1) given by

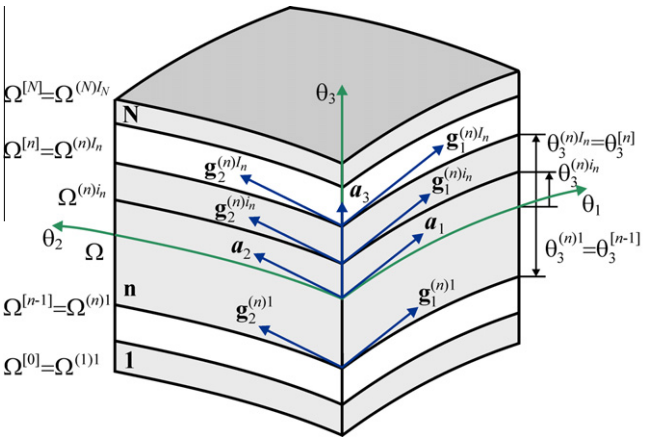

Fig. 1. Geometry of the laminated shell.

Table 1
Elastic, piezoelectric and dielectric properties of materials.[a]

Material	PZT-4	PZT-5	$(Pb, Ca)(Co_{1/2}W_{1/2})TiO_3$	Gr/Ep
C_{1111}, GPa	139.0	120.0	150.0	183.443
C_{2222}, GPa	139.0	120.0	150.0	11.662
C_{3333}, GPa	115.0	111.0	128.0	11.662
C_{1122}, GPa	77.8	75.2	37.1	4.363
C_{1133}, GPa	74.3	75.1	32.3	4.363
C_{2233}, GPa	74.3	75.1	32.3	3.918
C_{2323}, GPa	25.6	21.1	55.2	2.87
C_{1313}, GPa	25.6	21.1	55.2	7.17
C_{1212}, GPa	30.6	22.6	56.5	7.17
e_{311}, C/m^2	−5.2	−5.35	1.61	0
e_{322}, C/m^2	−5.2	−5.35	1.61	0
e_{333}, C/m^2	15.08	15.78	8.5	0
e_{223}, C/m^2	12.72			0
e_{113}, C/m^2	12.72			0
$\in_{11}/\in_0$	1475	1730	238	1728
$\in_{22}/\in_0$	1475	1730	238	1728
$\in_{33}/\in_0$	1300	1700	209	1728

[a] Vacuum permittivity $\in_0 = 8.854$ pF/m.

$$\mathbf{g}_\alpha^{(n)i_n} = \mathbf{R}_{,\alpha}^{(n)i_n} = A_\alpha c_\alpha^{(n)i_n}\mathbf{e}_\alpha, \quad \mathbf{g}_3^{(n)i_n} = \mathbf{e}_3, \tag{4}$$

where $c_\alpha^{(n)i_n} = 1 + k_\alpha \theta_3^{(n)i_n}$ are the components of the shifter tensor at SaS.

Here and in the following developments, $(\ldots)_{,i}$ stands for the partial derivatives with respect to coordinates θ_i; the index n identifies the belonging of any quantity to the nth layer and runs from 1 to N, where N is the number of layers; the index m_n identifies the belonging of any quantity to the inner SaS of the nth layer and runs from 2 to $I_n - 1$, whereas the indices i_n, j_n, k_n describe all SaS of the nth layer and run from 1 to I_n; Greek indices $\alpha,\ \beta$ range from 1 to 2; Latin indices $i,\ j,\ k,\ l$ range from 1 to 3.

Remark 1. As can be seen from Eq. (2), the transverse coordinates of inner SaS coincide with coordinates of Chebyshev polynomial nodes (see, e.g. Burden and Faires, 2010). This fact has a great meaning for a convergence of the SaS method (Kulikov and Plotnikova, 2012b, 2013a).

3. Kinematic description of deformed laminated shell

A position vector of the deformed shell is written as

$$\overline{\mathbf{R}} = \mathbf{R} + \mathbf{u}, \tag{5}$$

where $\mathbf{u}$ is the displacement vector, which is always measured in accordance with the total Lagrangian formulation from the initial configuration to the current configuration directly. In particular, the position vectors of SaS of the nth layer are

$$\overline{\mathbf{R}}^{(n)i_n} = \mathbf{R}^{(n)i_n} + \mathbf{u}^{(n)i_n}, \tag{6}$$

$$\mathbf{u}^{(n)i_n} = \mathbf{u}(\theta_3^{(n)i_n}), \tag{7}$$

where $\mathbf{u}^{(n)i_n}(\theta_1, \theta_2)$ are the displacement vectors of SaS of the nth layer.

The base vectors in the current shell configuration are defined as

$$\overline{\mathbf{g}}_i = \overline{\mathbf{R}}_{,i} = \mathbf{g}_i + \mathbf{u}_{,i}. \tag{8}$$

In particular, the base vectors of deformed SaS of the nth layer are

$$\overline{\mathbf{g}}_\alpha^{(n)i_n} = \overline{\mathbf{R}}_{,\alpha}^{(n)i_n} = \mathbf{g}_\alpha^{(n)i_n} + \mathbf{u}_{,\alpha}^{(n)i_n}, \quad \overline{\mathbf{g}}_3^{(n)i_n} = \overline{\mathbf{g}}_3(\theta_3^{(n)i_n}) = \mathbf{e}_3 + \boldsymbol{\beta}^{(n)i_n}, \tag{9}$$

$$\boldsymbol{\beta}^{(n)i_n} = \mathbf{u}_{,3}(\theta_3^{(n)i_n}), \tag{10}$$

Table 2
Results for a piezoelectric three-layer shell with $S = 2$ under mechanical loading.

I_n	$\bar{u}_1(-0.5)$	$\bar{u}_2(-0.5)$	$\bar{u}_3(-0.5)$	$\bar{\varphi}\,(0)$	$\bar{\sigma}_{11}(-0.5)$	$\bar{\sigma}_{22}(-0.5)$	$\bar{\sigma}_{12}(-0.5)$	$\bar{\sigma}_{13}(0)$	$\bar{\sigma}_{23}(0)$	$\bar{\sigma}_{33}(0)$	$\bar{D}_3(0)$
3	251.59	−539.53	740.23	2.8488	−14.325	−136.36	−82.661	56.821	−40.713	40.494	15.226
5	254.32	−543.71	742.09	2.8509	−13.457	−127.94	−83.397	57.592	−41.214	42.251	15.986
7	254.30	−543.65	742.07	2.8511	−13.433	−127.70	−83.389	57.589	−41.210	42.247	15.975
9	254.30	−543.65	742.07	2.8511	−13.431	−127.67	−83.389	57.589	−41.210	42.247	15.975
11	254.30	−543.65	742.07	2.8511	−13.430	−127.67	−83.389	57.589	−41.210	42.247	15.975

Table 3
Results for a piezoelectric three-layer shell with $S = 10$ under mechanical loading.

I_n	$\bar{u}_1(-0.5)$	$\bar{u}_2(-0.5)$	$\bar{u}_3(-0.5)$	$\bar{\varphi}\,(0)$	$\bar{\sigma}_{11}(-0.5)$	$\bar{\sigma}_{22}(-0.5)$	$\bar{\sigma}_{12}(-0.5)$	$\bar{\sigma}_{13}(0)$	$\bar{\sigma}_{23}(0)$	$\bar{\sigma}_{33}(0)$	$\bar{D}_3(0)$
3	139.73	−394.89	1025.5	0.17792	−4.4670	−1.7736	−47.463	5.3539	−3.1690	1.6908	−7.4562
5	139.73	−394.89	1025.5	0.17792	−4.4660	−1.5634	−47.464	5.4440	−3.2214	1.6555	−7.4493
7	139.73	−394.89	1025.5	0.17792	−4.4660	−1.5638	−47.464	5.4440	−3.2214	1.6555	−7.4493
9	139.73	−394.89	1025.5	0.17792	−4.4660	−1.5637	−47.464	5.4440	−3.2214	1.6555	−7.4493

where $\boldsymbol{\beta}^{(n)i_n}(\theta_1,\theta_2)$ are the values of the derivative of the 3D displacement vector with respect to coordinate θ_3 at SaS.

The Green–Lagrange strain tensor in an orthogonal curvilinear coordinate system can be written as

$$2\varepsilon_{ij} = \frac{1}{A_iA_jc_ic_j}(\bar{\mathbf{g}}_i\cdot\bar{\mathbf{g}}_j - \mathbf{g}_i\cdot\mathbf{g}_j), \tag{11}$$

where $A_3 = 1$ and $c_3 = 1$. In particular, the Green–Lagrange strains at SaS are

$$2\varepsilon_{ij}^{(n)i_n} = 2\varepsilon_{ij}(\theta_3^{(n)i_n}) = \frac{1}{A_iA_jc_i^{(n)i_n}c_j^{(n)i_n}}(\bar{\mathbf{g}}_i^{(n)i_n}\cdot\bar{\mathbf{g}}_j^{(n)i_n} - \mathbf{g}_i^{(n)i_n}\cdot\mathbf{g}_j^{(n)i_n}). \tag{12}$$

Substituting Eqs. (4) and (9) into the strain–displacement relationships (12) and discarding the non-linear terms, one obtains

$$2\varepsilon_{\alpha\beta}^{(n)i_n} = \frac{1}{A_\alpha c_\alpha^{(n)i_n}}\mathbf{u}_{,\alpha}^{(n)i_n}\cdot\mathbf{e}_\beta + \frac{1}{A_\beta c_\beta^{(n)i_n}}\mathbf{u}_{,\beta}^{(n)i_n}\cdot\mathbf{e}_\alpha,$$

$$2\varepsilon_{\alpha3}^{(n)i_n} = \boldsymbol{\beta}^{(n)i_n}\cdot\mathbf{e}_\alpha + \frac{1}{A_\alpha C_\alpha^{(n)i_n}}\mathbf{u}_{,\alpha}^{(n)i_n}\cdot\mathbf{e}_3, \varepsilon_{33}^{(n)i_n} = \boldsymbol{\beta}^{(n)i_n}\cdot\mathbf{e}_3. \tag{13}$$

Next, we represent the displacement vectors $\mathbf{u}^{(n)i_n}$ and $\boldsymbol{\beta}^{(n)i_n}$ in the reference surface frame $\mathbf{e}_i$ as follows:

$$\mathbf{u}^{(n)i_n} = \sum_i u_i^{(n)i_n}\mathbf{e}_i, \tag{14}$$

$$\boldsymbol{\beta}^{(n)i_n} = \sum_i \beta_i^{(n)i_n}\mathbf{e}_i. \tag{15}$$

Using (14) and well-known formulas for the derivatives of unit vectors $\mathbf{e}_i$ with respect to orthogonal curvilinear coordinates (Kulikov and Plotnikova, 2012b, 2013a), we have

$$\frac{1}{A_\alpha}\mathbf{u}_{,\alpha}^{(n)i_n} = \sum_i \lambda_{i\alpha}^{(n)i_n}\mathbf{e}_i, \tag{16}$$

where

$$\lambda_{\alpha\alpha}^{(n)i_n} = \frac{1}{A_\alpha}u_{\alpha,\alpha}^{(n)i_n} + B_\alpha u_\beta^{(n)i_n} + k_\alpha u_3^{(n)i_n},$$

$$\lambda_{\beta\alpha}^{(n)i_n} = \frac{1}{A_\alpha}u_{\beta,\alpha}^{(n)i_n} - B_\alpha u_\alpha^{(n)i_n} \quad \text{for} \quad \beta\neq\alpha,$$

$$\lambda_{3\alpha}^{(n)i_n} = \frac{1}{A_\alpha}u_{3,\alpha}^{(n)i_n} - k_\alpha u_\alpha^{(n)i_n}, \quad B_\alpha = \frac{1}{A_\alpha A_\beta}A_{\alpha,\beta} \quad \text{for} \quad \beta\neq\alpha. \tag{17}$$

Substitution of presentations (15) and (16) into the strain–displacement relationships (13) yields the component form of these relationships

$$2\varepsilon_{\alpha\beta}^{(n)i_n} = \frac{1}{c_\beta^{(n)i_n}}\lambda_{\alpha\beta}^{(n)i_n} + \frac{1}{c_\alpha^{(n)i_n}}\lambda_{\beta\alpha}^{(n)i_n},$$

$$2\varepsilon_{\alpha3}^{(n)i_n} = \beta_\alpha^{(n)i_n} + \frac{1}{c_\alpha^{(n)i_n}}\lambda_{3\alpha}^{(n)i_n}, \quad \varepsilon_{33}^{(n)i_n} = \beta_3^{(n)i_n}. \tag{18}$$

Up to this moment, no assumptions concerning displacement and strain fields have been made. We start now with the *first fundamental assumption* of the proposed shell formulation. Let us assume that the displacements are distributed through the thickness of the nth layer as follows:

$$u_i^{(n)} = \sum_{i_n} L^{(n)i_n}u_i^{(n)i_n}, \quad \theta_3^{[n-1]} \leqslant \theta_3 \leqslant \theta_3^{[n]}, \tag{19}$$

where $L^{(n)i_n}(\theta_3)$ are the Lagrange polynomials of degree $I_n - 1$ expressed as

$$L^{(n)i_n} = \prod_{j_n\neq i_n}\frac{\theta_3 - \theta_3^{(n)j_n}}{\theta_3^{(n)i_n} - \theta_3^{(n)j_n}}. \tag{20}$$

The use of Eqs. (10), (15), and (19) yields

$$\beta_i^{(n)i_n} = \sum_{j_n} M^{(n)j_n}(\theta_3^{(n)i_n})u_i^{(n)j_n}, \tag{21}$$

where $M^{(n)j_n} = L_3^{(n)j_n}$ are the derivatives of Lagrange polynomials. The values of these derivatives at SaS are calculated as

$$M^{(n)j_n}(\theta_3^{(n)i_n}) = \frac{1}{\theta_3^{(n)j_n} - \theta_3^{(n)i_n}}\prod_{k_n\neq i_n,j_n}\frac{\theta_3^{(n)i_n} - \theta_3^{(n)k_n}}{\theta_3^{(n)j_n} - \theta_3^{(n)k_n}} \quad \text{for } j_n\neq i_n,$$

$$M^{(n)i_n}(\theta_3^{(n)i_n}) = -\sum_{j_n\neq i_n} M^{(n)j_n}(\theta_3^{(n)i_n}). \tag{22}$$

So, the key functions $\beta_i^{(n)i_n}$ of the laminated shell formulation are represented according to (21) as a linear combination of displacements of SaS of the nth layer $u_i^{(n)j_n}$.

The following step consists in a choice of the correct approximation of strains through the thickness of the nth layer. It is apparent that the strain distribution should be chosen similar to the displacement distribution (19). Thus, the *second fundamental assumption* of the developed shell formulation can be written as

$$\varepsilon_{ij}^{(n)} = \sum_{i_n} L^{(n)i_n}\varepsilon_{ij}^{(n)i_n}, \quad \theta_3^{[n-1]} \leqslant \theta_3 \leqslant \theta_3^{[n]}. \tag{23}$$

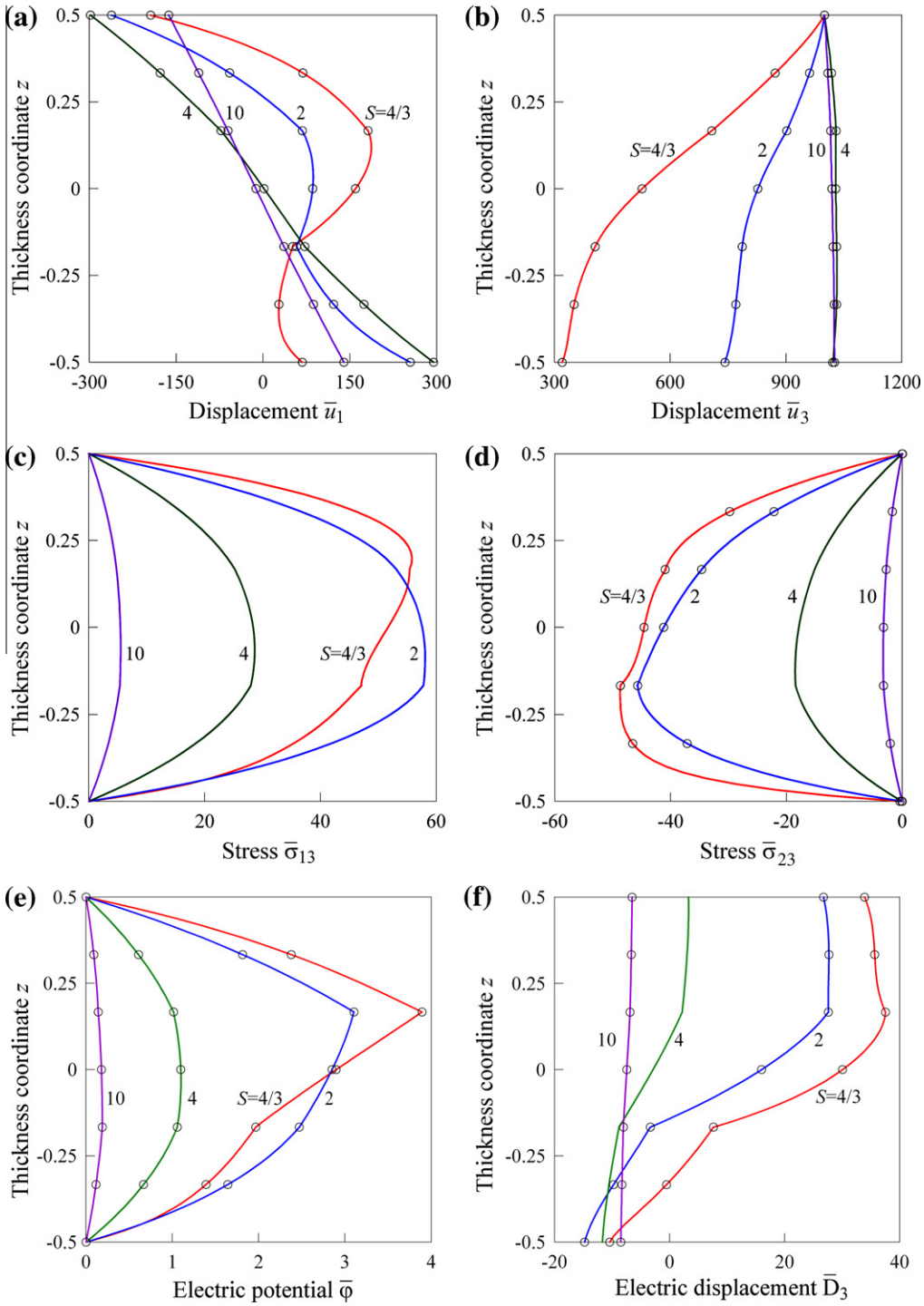

Fig. 2. Distributions of displacements, transverse shear stresses, electric potential and electric displacement through the thickness of the three-layer shell under mechanical loading for $I_1 = I_2 = I_3 = 7$: present analysis (——) and Heyliger (○).

Remark 2. Strain-displacement relationships (18) and (23) exactly represent all rigid-body motions of a laminated shell in any convected curvilinear coordinate system. The proof of this statement is given by Kulikov and Plotnikova (2013a).

4. Description of electric field

The relation between the electric field and the electric potential φ is given by

$$E_i = -\frac{1}{A_i c_i}\varphi_{,i}. \tag{24}$$

In particular, the electric field vector at SaS of the nth layer is presented as

$$E_\alpha^{(n)i_n} = E_\alpha(\theta_3^{(n)i_n}) = -\frac{1}{A_\alpha c_\alpha^{(n)i_n}}\varphi_{,\alpha}^{(n)i_n}, \tag{25}$$

$$E_3^{(n)i_n} = E_3(\theta_3^{(n)i_n}) = -\psi^{(n)i_n}, \tag{26}$$

Table 4
Results for a piezoelectric three-layer shell with $S = 2$ under electric loading.

I_n	$\bar{u}_1(-0.5)$	$\bar{u}_2(-0.5)$	$\bar{u}_3(-0.5)$	$\bar{\varphi}\ (0)$	$\bar{\sigma}_{11}(-0.5)$	$\bar{\sigma}_{22}(-0.5)$	$\bar{\sigma}_{12}(-0.5)$	$\bar{\sigma}_{13}(0)$	$\bar{\sigma}_{23}(0)$	$\bar{\sigma}_{33}(0)$	$\bar{D}_3(0)$
3	−8.0471	16.158	−0.64421	2.6894	−1.5080	−12.751	2.5383	7.5733	−6.5742	0.8436	−37.197
5	−7.9780	16.144	−0.59556	2.6878	−1.6051	−13.706	2.5285	8.0537	−6.9389	1.1103	−36.807
7	−7.9778	16.143	−0.59384	2.6879	−1.6021	−13.676	2.5283	8.0504	−6.9365	1.1176	−36.808
9	−7.9778	16.143	−0.59384	2.6879	−1.6026	−13.681	2.5283	8.0503	−6.9365	1.1175	−36.808
11	−7.9778	16.143	−0.59384	2.6879	−1.6026	−13.681	2.5283	8.0503	−6.9365	1.1175	−36.808

Table 5
Results for a piezoelectric three-layer shell with $S = 10$ under electric loading.

I_n	$\bar{u}_1(-0.5)$	$\bar{u}_2(-0.5)$	$\bar{u}_3(-0.5)$	$\bar{\varphi}\ (0)$	$\bar{\sigma}_{11}(-0.5)$	$\bar{\sigma}_{22}(-0.5)$	$\bar{\sigma}_{12}(-0.5)$	$\bar{\sigma}_{13}(0)$	$\bar{\sigma}_{23}(0)$	$\bar{\sigma}_{33}(0)$	$\bar{D}_3(0)$
3	−216.19	−315.58	1664.6	5.2389	−121.24	−925.26	−156.36	9.9160	−5.8683	−1.5371	−221.36
5	−216.19	−315.59	1664.7	5.2389	−121.48	−927.68	−156.38	10.111	−5.9792	−1.5454	−221.21
7	−216.19	−315.59	1664.7	5.2389	−121.48	−927.67	−156.38	10.111	−5.9791	−1.5453	−221.21
9	−216.19	−315.59	1664.7	5.2389	−121.48	−927.67	−156.38	10.111	−5.9791	−1.5453	−221.21

where $\varphi^{(n)i_n}(\theta_1,\theta_2)$ are the electric potentials of SaS of the nth layer; $\psi^{(n)i_n}(\theta_1,\theta_2)$ are the values of the derivative of the electric potential with respect to thickness coordinate θ_3 at SaS, that is,

$$\varphi^{(n)i_n} = \varphi(\theta_3^{(n)i_n}), \quad \psi^{(n)i_n} = \varphi_{,3}(\theta_3^{(n)i_n}). \tag{27}$$

Now, we accept the *third fundamental assumption* of the proposed piezoelectric shell formulation concerning the electric potential and the electric field vector, which are distributed through the thickness of the nth layer as follows:

$$\varphi^{(n)} = \sum_{i_n} L^{(n)i_n}\varphi^{(n)i_n}, \quad \theta_3^{[n-1]} \leqslant \theta_3 \leqslant \theta_3^{[n]}, \tag{28}$$

$$E_i^{(n)} = \sum_{i_n} L^{(n)i_n}E_i^{(n)i_n}, \quad \theta_3^{[n-1]} \leqslant \theta_3 \leqslant \theta_3^{[n]}. \tag{29}$$

The use of Eqs. (27) and (28) leads to a simple formula

$$\psi^{(n)i_n} = \sum_{j_n} M^{(n)j_n}(\theta_3^{(n)i_n})\varphi^{(n)j_n}, \tag{30}$$

which is similar to (21). This implies that the key functions $\psi^{(n)i_n}$ of the piezoelectric shell formulation are represented as a linear combination of electric potentials of SaS of the nth layer $\varphi^{(n)j_n}$.

5. Variational formulation

The variational equation for the piezoelectric laminated shell in the case of conservative loading can be written as

$$\delta\Pi = 0, \tag{31}$$

where Π is the extended potential energy (Tzou, 1993) defined as

$$\Pi = \frac{1}{2}\int\int_\Omega \sum_n \int_{\theta_3^{[n-1]}}^{\theta_3^{[n]}} \left(\sum_{i,j}\sigma_{ij}^{(n)}\varepsilon_{ij}^{(n)} - \sum_i D_i^{(n)}E_i^{(n)}\right) A_1A_2c_1c_2\,d\theta_2\,d\theta_3 - W, \tag{32}$$

$$W = \int\int_\Omega \left(\sum_i p_i^+ u_i^{[N]} - q^+\phi^{[N]}\right) A_1A_2c_1^{[N]}c_2^{[N]}\,d\theta_1\,d\theta_2 - \int\int_\Omega \left(\sum_i p_i^- u_i^{[0]} - q^-\varphi^{[0]}\right) A_1A_2c_1^{[0]}c_2^{[0]}\,d\theta_1\,d\theta_2 + W_\Sigma, \tag{33}$$

where $\sigma_{ij}^{(n)}$ is the stress tensor of the nth layer; $D_i^{(n)}$ is the electric displacement vector of the nth layer; $u_i^{[0]} = u_i^{(1)1}$ and $u_i^{[N]} = u_i^{(N)I_N}$ are the displacements of bottom and top surfaces $\Omega^{[0]}$ and $\Omega^{[N]}$; $\varphi^{[0]} = \varphi^{(1)1}$ and $\varphi^{[N]} = \varphi^{(N)I_N}$ are the electric potentials of bottom and top surfaces; $c_\alpha^{[0]} = 1 + k_\alpha\theta_3^{[0]}$ and $c_\alpha^{[N]} = 1 + k_\alpha\theta_3^{[N]}$ are the components of the shifter tensor at outer surfaces; p_i^- and p_i^+ are the loads acting on outer surfaces; q^- and q^+ are the electric charges on outer surfaces; W_Σ is the work done by external electromechanical loads applied to the boundary surface Σ.

Substituting strain and electric field distributions (23) and (29) in Eq. (32) and introducing stress resultants

$$H_{ij}^{(n)i_n} = \int_{\theta_3^{[n-1]}}^{\theta_3^{[n]}} \sigma_{ij}^{(n)}L^{(n)i_n}c_1c_2\,d\theta_3 \tag{34}$$

and electric displacement resultants

$$T_i^{(n)i_n} = \int_{\theta_3^{[n-1]}}^{\theta_3^{[n]}} D_i^{(n)}L^{(n)i_n}c_1c_2\,d\theta_3, \tag{35}$$

one obtains

$$\Pi = \frac{1}{2}\int\int_\Omega \sum_n\sum_{i_n}\left(\sum_{i,j}H_{ij}^{(n)i_n}\varepsilon_{ij}^{(n)i_n} - \sum_i T_i^{(n)i_n}E_i^{(n)i_n}\right)A_1A_2\,d\theta_1\,d\theta_2 - W. \tag{36}$$

For simplicity, we consider the case of linear piezoelectric materials described as

$$\sigma_{ij}^{(n)} = \sum_{k,\ell} C_{ijk\ell}^{(n)}\varepsilon_{k\ell}^{(n)} - \sum_k e_{kij}^{(n)}E_k^{(n)}, \quad \theta_3^{[n-1]} \leqslant \theta_3 \leqslant \theta_3^{[n]}, \tag{37}$$

$$D_i^{(n)} = \sum_{k,\ell} e_{ik\ell}^{(n)}\varepsilon_{k\ell}^{(n)} + \sum_k \in_{ik}^{(n)}E_k^{(n)}, \quad \theta_3^{[n-1]} \leqslant \theta_3 \leqslant \theta_3^{[n]}, \tag{38}$$

where $C_{ijkl}^{(n)}$, $e_{kij}^{(n)}$ and $\in_{ik}^{(n)}$ are the elastic, piezoelectric and dielectric constants of the nth layer.

Inserting (37) and (38) correspondingly in Eqs. (34) and (35) and allowing for strain and electric field distributions (23) and (29), we arrive at needed formulas for stress and electric displacement resultants

$$H_{ij}^{(n)i_n} = \sum_{j_n}\Lambda^{(n)i_nj_n}\left(\sum_{k,\ell}C_{ijk\ell}^{(n)}\varepsilon_{k\ell}^{(n)j_n} - \sum_k e_{kij}^{(n)}E_k^{(n)j_n}\right), \tag{39}$$

$$T_i^{(n)i_n} = \sum_{j_n}\Lambda^{(n)i_nj_n}\left(\sum_{k,\ell}e_{ik\ell}^{(n)}\varepsilon_{k\ell}^{(n)j_n} + \sum_k \in_{ik}^{(n)}E_k^{(n)j_n}\right), \tag{40}$$

where

$$\Lambda^{(n)i_nj_n} = \int_{\theta_3^{[n-1]}}^{\theta_3^{[n]}} L^{(n)i_n}L^{(n)j_n}c_1c_2\,d\theta_3. \tag{41}$$

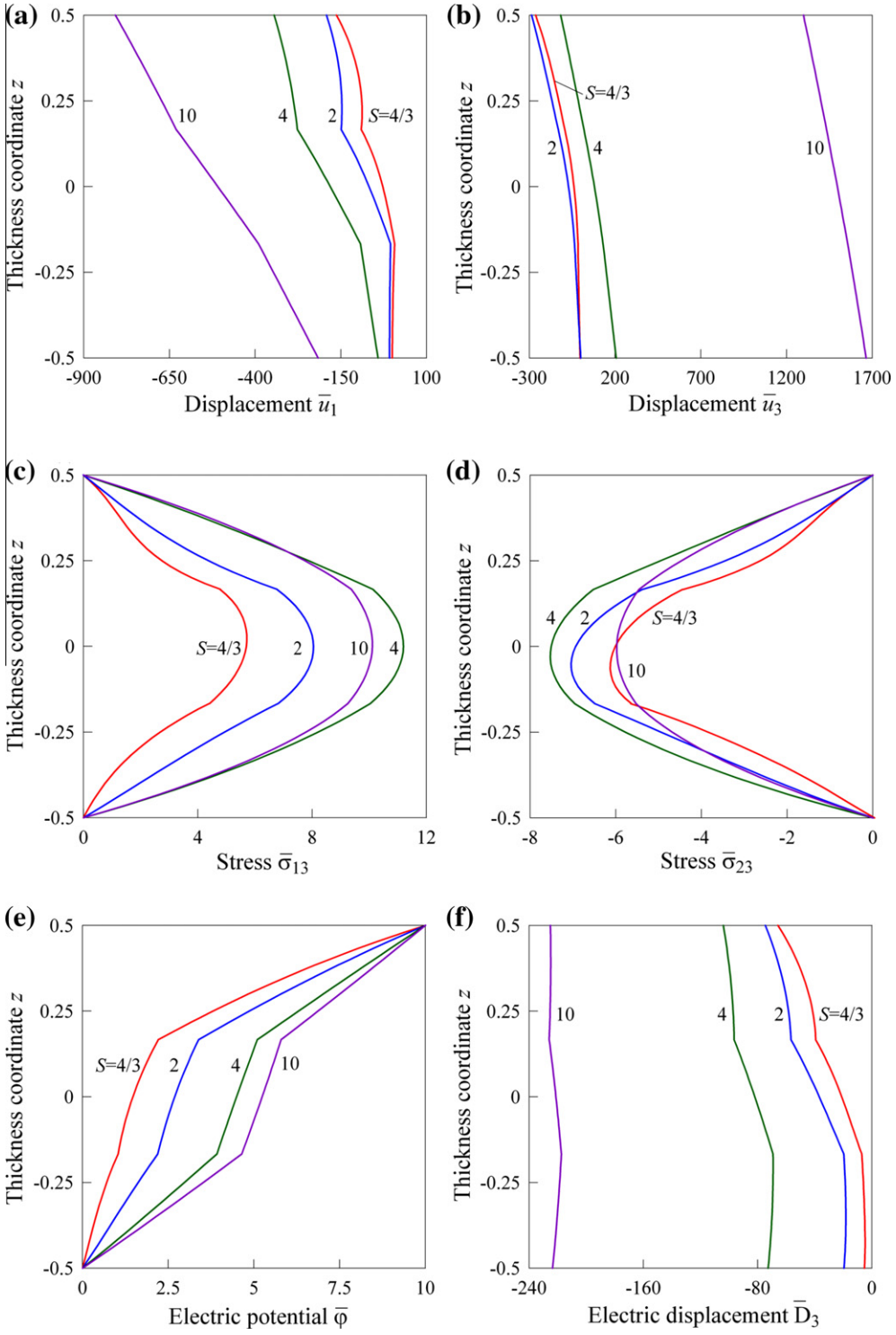

Fig. 3. Distributions of displacements, transverse shear stresses, electric potential and electric displacement through the thickness of the three-layer shell under electric loading for $I_1 = I_2 = I_3 = 7$.

Table 6
Results for an angle-ply shell with $R/h = 2$ under mechanical loading.

I_n	$\bar{u}_1(-0.5)$	$\bar{u}_2(-0.5)$	$\bar{u}_3$ (0)	$\bar{\varphi}(-0.5)$	$\bar{\sigma}_{11}(-0.5)$	$\bar{\sigma}_{22}(-0.5)$	$\bar{\sigma}_{12}(-0.5)$	$\bar{\sigma}_{13}(-0.125)$	$\bar{\sigma}_{23}(0.125)$	$\bar{\sigma}_{33}(0.125)$	$\bar{D}_3(0.25)$
3	1.0761	1.5908	2.4725	2.1609	−2.4302	1.2751	−1.5292	39.469	−5.0190	60.729	−2.3067
5	1.0771	1.5916	2.4738	2.1510	−2.3994	1.3090	−1.5301	39.888	−5.9840	60.613	−2.3636
7	1.0771	1.5916	2.4738	2.1511	−2.3994	1.3090	−1.5301	39.884	−5.9738	60.614	−2.3636
9	1.0771	1.5916	2.4738	2.1511	−2.3993	1.3090	−1.5301	39.884	−5.9738	60.614	−2.3636

Table 7
Results for an angle-ply shell with $R/h = 10$ under mechanical loading.

I_n	$\bar{u}_1(-0.5)$	$\bar{u}_2(-0.5)$	$\bar{u}_3$ (0)	$\bar{\varphi}(-0.5)$	$\bar{\sigma}_{11}(-0.5)$	$\bar{\sigma}_{22}(-0.5)$	$\bar{\sigma}_{12}(-0.5)$	$\bar{\sigma}_{13}(-0.125)$	$\bar{\sigma}_{23}(0.125)$	$\bar{\sigma}_{33}(0.125)$	$\bar{D}_3(0.25)$
3	5.1521	−1.5498	16.792	8.7690	−9.2231	11.503	1.4899	48.534	−11.879	58.679	−18.308
5	5.1521	−1.5498	16.792	8.7689	−9.2127	11.514	1.4899	49.165	−12.305	60.677	−18.316
7	5.1521	−1.5498	16.792	8.7689	−9.2127	11.514	1.4899	49.165	−12.305	60.677	−18.316

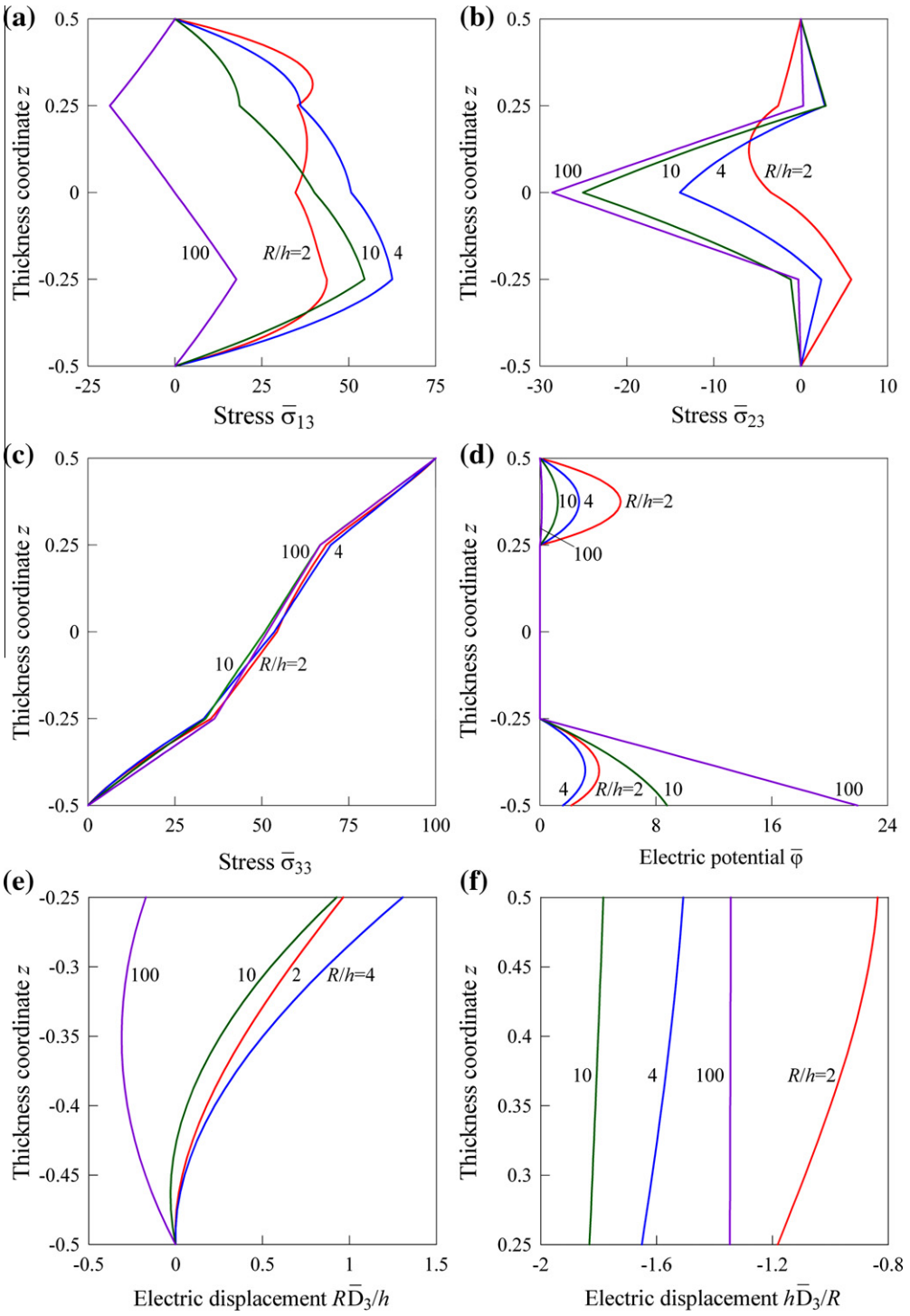

Fig. 4. Distributions of transverse stresses, electric potential and electric displacement in the thickness direction of the angle-ply cylindrical shell under mechanical loading for $I_1 = I_2 = I_3 = I_4 = 7$.

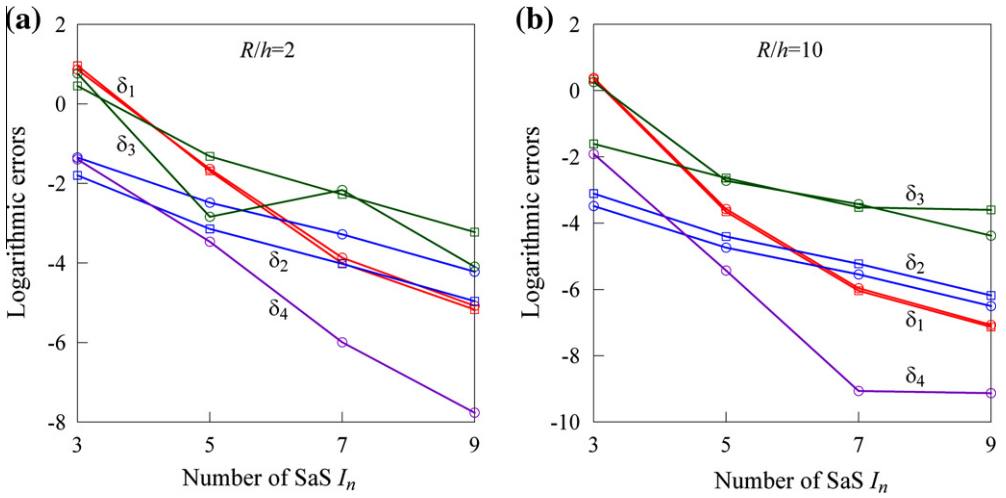

Fig. 5. Accuracy of satisfying the boundary conditions δ_i^-, δ_4^- and δ_i^+ on the bottom (○) and top (□) surfaces of the angle-ply cylindrical shell under mechanical loading.

Table 8
Results for an angle-ply shell with $R/h = 2$ under electric loading.

I_n	$\bar{u}_1(-0.5)$	$\bar{u}_2(-0.5)$	$\bar{u}_3$ (0)	$\bar{\varphi}(-0.5)$	$\bar{\sigma}_{11}(-0.5)$	$\bar{\sigma}_{22}(-0.5)$	$\bar{\sigma}_{12}(-0.5)$	$\bar{\sigma}_{13}(-0.125)$	$\bar{\sigma}_{23}(0.125)$	$\bar{\sigma}_{33}(0.125)$	$\bar{D}_3(0.25)$
3	1.3870	1.8170	3.3638	8.0105	−2.9838	1.9809	−1.7467	28.520	−2.2812	76.479	−126.22
5	1.3892	1.8199	3.3677	7.9784	−2.9523	2.0184	−1.7496	30.615	−5.3778	77.872	−128.18
7	1.3892	1.8199	3.3677	7.9784	−2.9523	2.0184	−1.7496	30.595	−5.3424	77.871	−128.18
9	1.3892	1.8199	3.3677	7.9784	−2.9523	2.0184	−1.7496	30.595	−5.3426	77.871	−128.18
11	1.3892	1.8199	3.3677	7.9784	−2.9522	2.0184	−1.7496	30.595	−5.3426	77.871	−128.18

Table 9
Results for an angle-ply shell with $R/h = 10$ under electric loading.

I_n	$\bar{u}_1(-0.5)$	$\bar{u}_2(-0.5)$	$\bar{u}_3$ (0)	$\bar{\varphi}(-0.5)$	$\bar{\sigma}_{11}(-0.5)$	$\bar{\sigma}_{22}(-0.5)$	$\bar{\sigma}_{12}(-0.5)$	$\bar{\sigma}_{13}(-0.125)$	$\bar{\sigma}_{23}(0.125)$	$\bar{\sigma}_{33}(0.125)$	$\bar{D}_3(0.25)$
3	0.98465	−4.6843	19.867	55.325	6.5317	21.436	4.5031	−116.34	−42.075	90.431	−603.13
5	0.98469	−4.6843	19.867	55.325	6.5276	21.433	4.5031	−115.22	−42.757	90.818	−603.50
7	0.98469	−4.6843	19.867	55.325	6.5276	21.433	4.5031	−115.22	−42.757	90.818	−603.50

Remark 3. The proposed 3D variational formulation generalizes 6- and 9- parameter formulations for piezoelectric shells based on the use of displacements of respectively two and three SaS (Kulikov and Plotnikova, 2008, 2011a).

6. 3D exact solution for piezoelectric orthotropic cylindrical shells

In this section, we study a simply supported piezoelectric laminated orthotropic cylindrical shell. Let the middle surface of the shell be described by axial and circumferential coordinates θ_1 and θ_2. The edge boundary conditions of the shell are assumed to be fully supported and electrically grounded, that is,

$$\sigma_{11}^{(n)} = u_2^{(n)} = u_3^{(n)} = \varphi^{(n)} = 0 \quad \text{at } \theta_1 = 0 \quad \text{and } \theta_1 = L, \tag{42}$$

where L is the length of the shell. To satisfy boundary conditions (42), we search an analytical solution of the problem by a method of double Fourier series expansion

$$\begin{aligned}
u_1^{(n)i_n} &= \sum_{r=1}^{\infty}\sum_{s=0}^{\infty} u_{1rs}^{(n)i_n} \cos\frac{r\pi\theta_1}{L}\cos s\theta_2,\\
u_2^{(n)i_n} &= \sum_{r=1}^{\infty}\sum_{s=0}^{\infty} u_{2rs}^{(n)i_n} \sin\frac{r\pi\theta_1}{L}\sin s\theta_2,\\
u_3^{(n)i_n} &= \sum_{r=1}^{\infty}\sum_{s=0}^{\infty} u_{3rs}^{(n)i_n} \sin\frac{r\pi\theta_1}{L}\cos s\theta_2,\\
\varphi^{(n)i_n} &= \sum_{r=1}^{\infty}\sum_{s=0}^{\infty} \varphi_{rs}^{(n)i_n} \sin\frac{r\pi\theta_1}{L}\cos s\theta_2.
\end{aligned} \tag{43}$$

The external electromechanical loads are also expanded in double Fourier series.

Substituting (43) and Fourier series corresponding to electromechanical loading in Eqs. (33) and (36) with $W_\Sigma = 0$ and allowing for relations (17), (18), (21), (25), (26), (30), (39), and (40), one finds

$$\Pi = \sum_{r=1}^{\infty}\sum_{s=0}^{\infty}\Pi_{rs}(u_{irs}^{(n)i_n}, \varphi_{rs}^{(n)i_n}). \tag{44}$$

Invoking further the variational equation (31), the following system of linear algebraic equations of order $4(\sum {}_nI_n - N + 1)$ is obtained:

$$\frac{\partial\Pi_{rs}}{\partial u_{irs}^{(n)i_n}} = 0, \quad \frac{\partial\Pi_{rs}}{\partial\varphi_{rs}^{(n)i_n}} = 0. \tag{45}$$

The linear system (45) can be easily solved by a method of Gaussian elimination.

The described algorithm was performed with the Symbolic Math Toolbox, which incorporates symbolic computations into the numeric environment of MATLAB. This gives the possibility to derive the exact solutions of 3D electroelasticity for laminated orthotropic cylindrical shells with a specified accuracy.

6.1. Piezoelectric three-layer cylindrical shell under mechanical loading

Consider a symmetric three-layer cylindrical shell with ply thicknesses $h_1 = h_2 = h_3 = h/3$ under an imposed transverse deformation

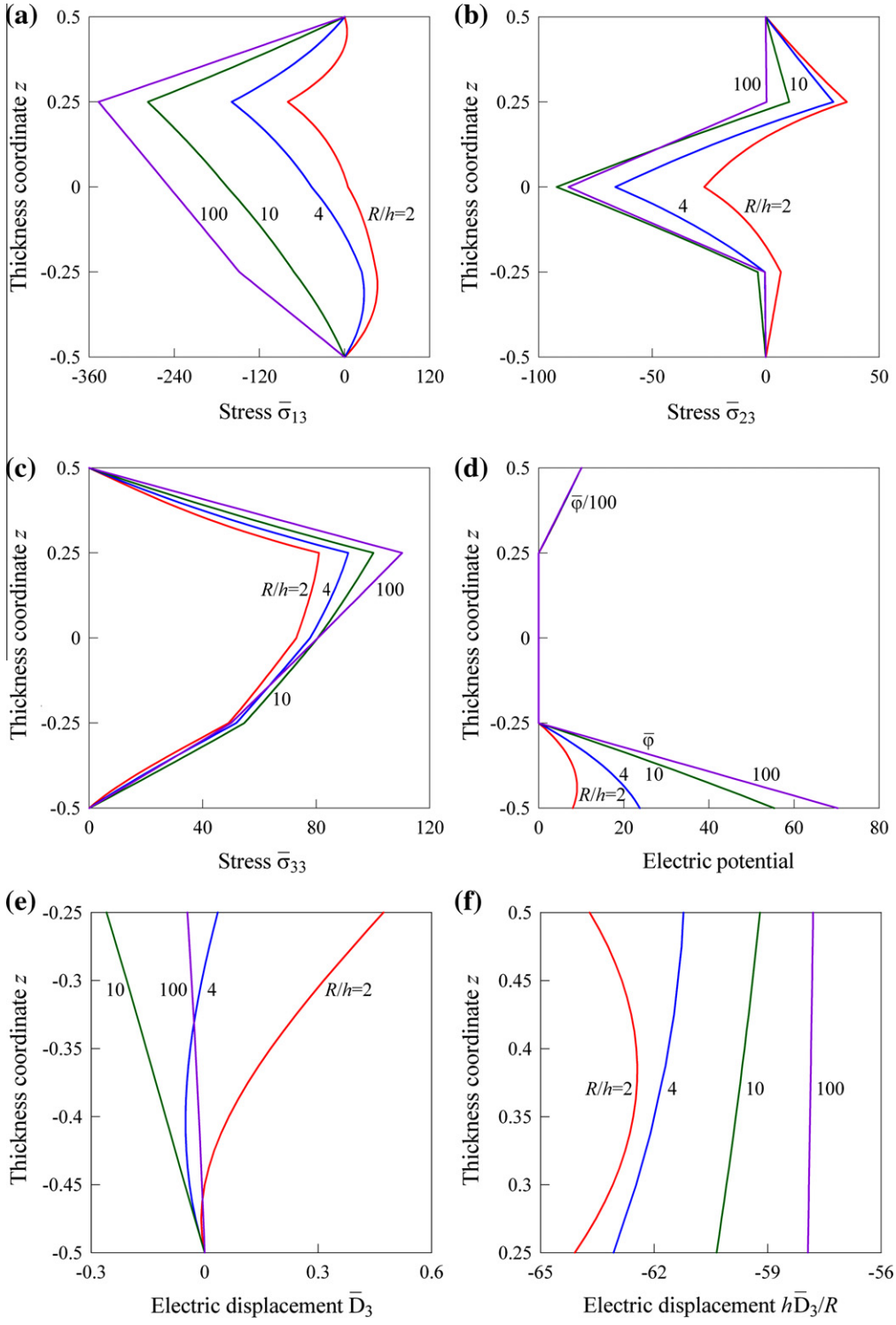

Fig. 6. Distributions of transverse stresses, electric potential and electric displacement in the thickness direction of the angle-ply cylindrical shell under electric loading for $I_1 = I_2 = I_3 = I_4 = 7$.

$$p_1^- = p_1^+ = p_2^- = p_2^+ = p_3^- = 0, \quad u_3^{[N]} = u_0 \sin\frac{\pi\theta_1}{L}\cos 2\theta_2. \tag{46}$$

The bottom and top layers are composed of PZT-4 with material properties given in Table 1. The middle layer is made of a fictitious material with the elastic constants exactly half of the PZT-4 and the piezoelectric and dielectric constants exactly double those of the PZT-4 (Heyliger, 1997). The both outer surfaces of the shell are assumed to be electrically grounded. To compare the results with an exact solution of Heyliger (1997), one has to fix $L = R^+ = 0.01$ m and $u_0 = 10^{-8}$ m, where R^+ is the radius of the top cylindrical surface. For the robust analysis it is convenient to introduce the following variables:

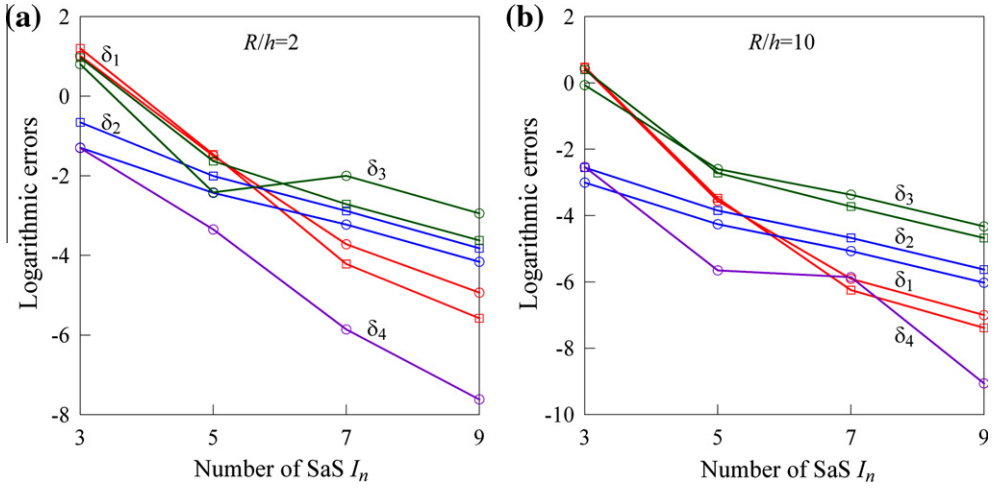

Fig. 7. Accuracy of satisfying the boundary conditions δ_i^-, δ_4^- and δ_i^+ on the bottom (○) and top (□) surfaces of the angle-ply cylindrical shell under electric loading.

Table 10
Results for a two-layer spherical shell with $R/h = 1.5$ under mechanical loading.

I_n	$10^{13} \times u_3$ (0)	$10^{13} \times u_3(0.5)$	$10^5 \times \varphi$ (0)	$\sigma_{11}(-0.5)$	$\sigma_{11}(0.5)$	$\sigma_{33}(-0.5)$	$\sigma_{33}(0.5)$	$10^5 \times D_3(-0.5)$	$10^5 \times D_3(0.5)$
3	1.2609	2.2609	−1.3557	0.81645	1.0028	1.1895	0.9854	18.166	4.5526
5	1.2626	2.2278	−1.3615	0.88583	1.0345	1.3005	0.9985	19.129	4.7833
7	1.2626	2.2278	−1.3616	0.88438	1.0378	1.2976	1.0002	19.145	4.7862
9	1.2626	2.2278	−1.3616	0.88485	1.0376	1.2984	1.0000	19.145	4.7862
11	1.2626	2.2278	−1.3616	0.88489	1.0376	1.2985	1.0000	19.145	4.7862
13	1.2626	2.2278	−1.3616	0.88490	1.0376	1.2985	1.0000	19.145	4.7862
Exact	1.26	2.23	−1.36						

$$\bar{u}_1 = 10^{11} \times u_1(0,0,z), \quad \bar{u}_2 = 10^{11} \times u_2(L/2,\pi/4,z),$$
$$\bar{u}_3 = 10^{11} \times u_3(L/2,0,z), \quad \bar{\sigma}_{11} = 10^{-4} \times \sigma_{11}(L/2,0,z),$$
$$\bar{\sigma}_{22} = 10^{-3} \times \sigma_{22}(L/2,0,z),$$
$$\bar{\sigma}_{33} = 10^{-3} \times \sigma_{33}(L/2,0,z),$$
$$\bar{\sigma}_{12} = 10^{-3} \times \sigma_{12}(0,\pi/4,z), \quad \bar{\sigma}_{13} = 10^{-3} \times \sigma_{13}(0,0,z),$$
$$\bar{\sigma}_{23} = 10^{-3} \times \sigma_{23}(L/2,\pi/4,z), \quad \bar{\varphi} = \varphi(L/2,0,z),$$
$$\bar{D}_3 = 10^6 \times D_3(L/2,0,z), \quad z = \theta_3/h. \tag{47}$$

The data listed in Tables 2 and 3 show that the SaS method permits one to find the 3D exact solution for thick piezoelectric laminated orthotropic shells with a prescribed accuracy by using a sufficiently large number of SaS denoted by I_n. Fig. 2 displays the distributions of displacements, transverse shear stresses, electric potential and electric displacement in the thickness direction for different values of the slenderness ratio $S = R^+/h$ employing seven SaS for each layer. These results demonstrate convincingly the high potential of the proposed piezoelectric shell formulation. This is due to the fact that boundary conditions on the bottom and top surfaces of the shell and continuity conditions at layer interfaces for transverse shear stresses are satisfied exactly, which are evaluated through the constitutive equations (37).

6.2. Piezoelectric three-layer cylindrical shell under electric loading

Consider next the same three-layer cylindrical shell with $L = R^+ = 0.01$ m subjected to electric loading

$$\varphi^{[0]} = 0, \quad \varphi^{[N]} = \varphi_0 \sin\frac{\pi\theta_1}{L}\cos 2\theta_2, \tag{48}$$

where $\varphi_0 = 10$ V. The bottom and top surfaces of the shell are assumed to be traction free.

Tables 4 and 5 demonstrate again the high potential of the piezoelectric laminated shell formulation developed. Fig. 3 shows the distributions of displacements, transverse shear stresses, electric potential and electric displacement in the thickness direction for different values of the slenderness ratio S employing seven SaS for each layer. It is seen that boundary conditions on the bottom and top surfaces of the shell and continuity conditions at layer interfaces for transverse shear stresses are fulfilled properly.

7. 3D exact solution for piezoelectric anisotropic cylindrical shells

Herein, we study a symmetric deformation of the simply supported piezoelectric laminated anisotropic shell. The boundary conditions of the shell with electrically grounded edges are taken as

$$\sigma_{11}^{(n)} = \sigma_{12}^{(n)} = u_3^{(n)} = \varphi^{(n)} = 0 \quad \text{at } \theta_1 = 0 \quad \text{and } \theta_1 = L \tag{49}$$

to simulate simple supports. In the case of a monoclinic piezoelectric material with poling direction coincident with the θ_3 axis, we can search an analytical solution of the problem as follows:

$$u_1^{(n)i_n} = \sum_{r=1}^{\infty} u_{1r}^{(n)i_n} \cos\frac{r\pi\theta_1}{L}, \quad u_2^{(n)i_n} = \sum_{r=1}^{\infty} u_{2r}^{(n)i_n} \cos\frac{r\pi\theta_1}{L},$$

$$u_3^{(n)i_n} = \sum_{r=1}^{\infty} u_{3r}^{(n)i_n} \sin\frac{r\pi\theta_1}{L}, \quad \varphi^{(n)i_n} = \sum_{r=1}^{\infty} \varphi_r^{(n)i_n} \sin\frac{r\pi\theta_1}{L}. \tag{50}$$

The external electromechanical loads are also expanded in Fourier series.

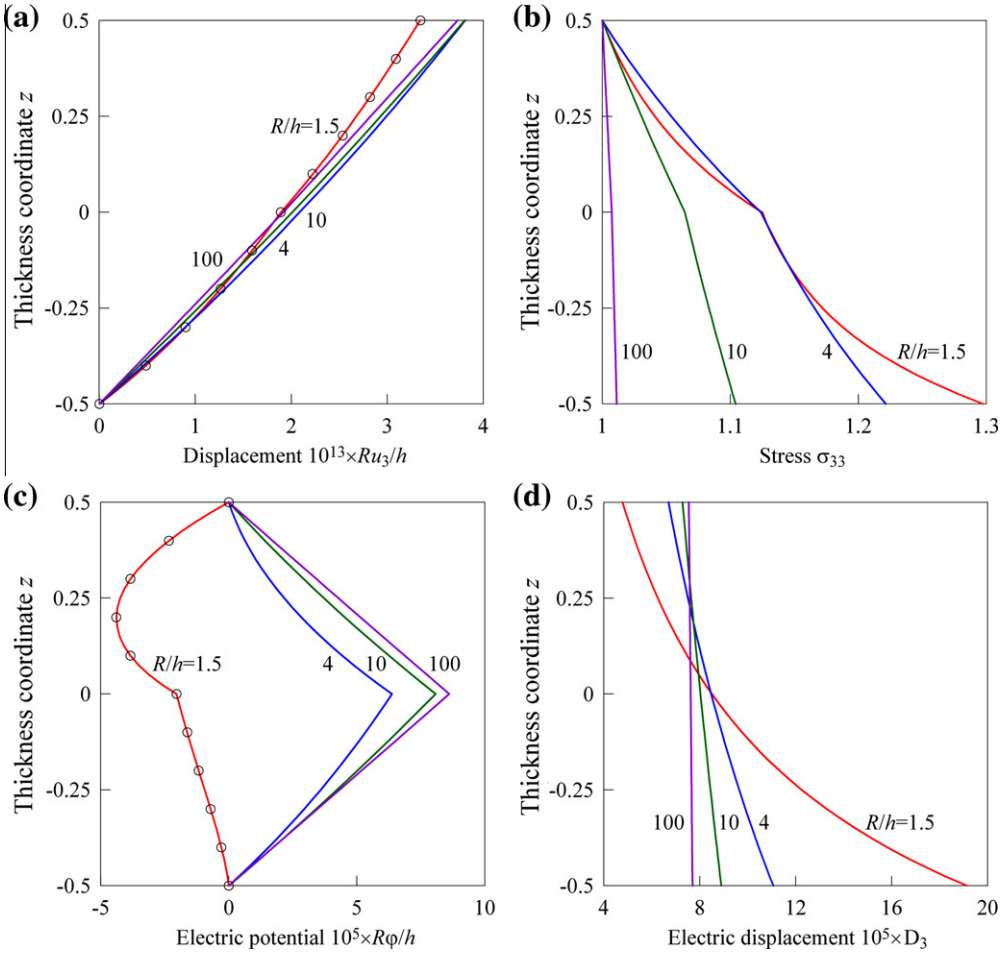

Fig. 8. Distributions of transverse displacement, transverse normal stress, electric potential and electric displacement in the thickness direction of the two-layer spherical shell under mechanical loading for $I_1 = I_2 = 7$: SaS method (——) and Heyliger and Wu (○).

Substituting (50) and Fourier series corresponding to electromechanical loading in Eqs. (33) and (36) and taking into account relations (17), (18), (21), (25), (26), (30), (39), and (40), one finds

$$\Pi = \sum_{r=1}^{\infty} \Pi_r(u_{ir}^{(n)i_n}, \varphi_r^{(n)i_n}). \tag{51}$$

The use of the variational equation (31) leads to a system of linear algebraic equations of order $4(\sum {}_nI_n - N + 1)$:

$$\frac{\partial \Pi_r}{\partial u_{ir}^{(n)i_n}} = 0, \quad \frac{\partial \Pi_r}{\partial \varphi_r^{(n)i_n}} = 0, \tag{52}$$

which is solved by a method of Gaussian elimination.

The described algorithm was performed with the Symbolic Math Toolbox, which incorporates symbolic computations into the numeric environment of MATLAB. This allows one to derive the exact solutions of 3D electroelasticity for piezoelectric anisotropic cylindrical shells with a specified accuracy.

7.1. Angle-ply shell with attached piezoelectric layers under mechanical loading

An angle-ply cylindrical shell with the stacking sequence [45/-45] is composed of the graphite-epoxy composite and covered with PZT-4 layers on its bottom and top surfaces. This means that a four-layer cylindrical shell [PZT/45/-45/PZT] is studied. The electromechanical properties of both materials are given in Table 1. The interfaces between the substrate and piezoelectric layers are electroded and grounded. The geometric parameters are taken to be $L = R = 0.1$ m and $h_n = h/4$, where R is the radius of the middle cylindrical surface and $n = 1, 2, 3, 4$.

The boundary conditions on the bottom and top surfaces are written as

$$\sigma_{13}^{[0]} = \sigma_{13}^{[N]} = \sigma_{23}^{[0]} = \sigma_{23}^{[N]} = \sigma_{33}^{[0]} = 0, \quad \sigma_{33}^{[N]} = p_0 \sin\frac{\pi\theta_1}{L},$$

$$D_3^{[0]} = 0, \quad \varphi^{[N]} = 0, \tag{53}$$

where $p_0 = 100$ Pa. To analyze the derived results for both types of loading efficiently, we introduce the following variables:

$$\begin{aligned}
&\bar{u}_1 = 10^{10} \times u_1(0,z), \quad \bar{u}_2 = 10^{11} \times u_2(0,z),\\
&\bar{u}_3 = 10^{10} \times u_3(L/2,z), \quad \bar{\sigma}_{11} = 10^{-2} \times \sigma_{11}(L/2,z),\\
&\bar{\sigma}_{22} = 10^{-2} \times \sigma_{22}(L/2,z), \quad \bar{\sigma}_{33} = \sigma_{33}(L/2,z),\\
&\bar{\sigma}_{12} = 10^{-1} \times \sigma_{12}(L/2,z), \quad \bar{\sigma}_{13} = \sigma_{13}(0,z),\\
&\bar{\sigma}_{23} = \sigma_{23}(0,z), \quad \bar{\varphi} = 10^{3} \times \varphi(L/2,z),\\
&\bar{D}_3 = 10^{8} \times D_3(L/2,z), \quad z = \theta_3/h.
\end{aligned} \tag{54}$$

The data from Tables 6 and 7 show that the SaS method gives the possibility to find the exact solution of 3D electroelasticity for thick angle-ply cylindrical shells with a prescribed accuracy using a sufficient number of SaS. Fig. 4 presents the distributions of the transverse stresses and electric potential through the thickness of a shell and the electric displacement through the

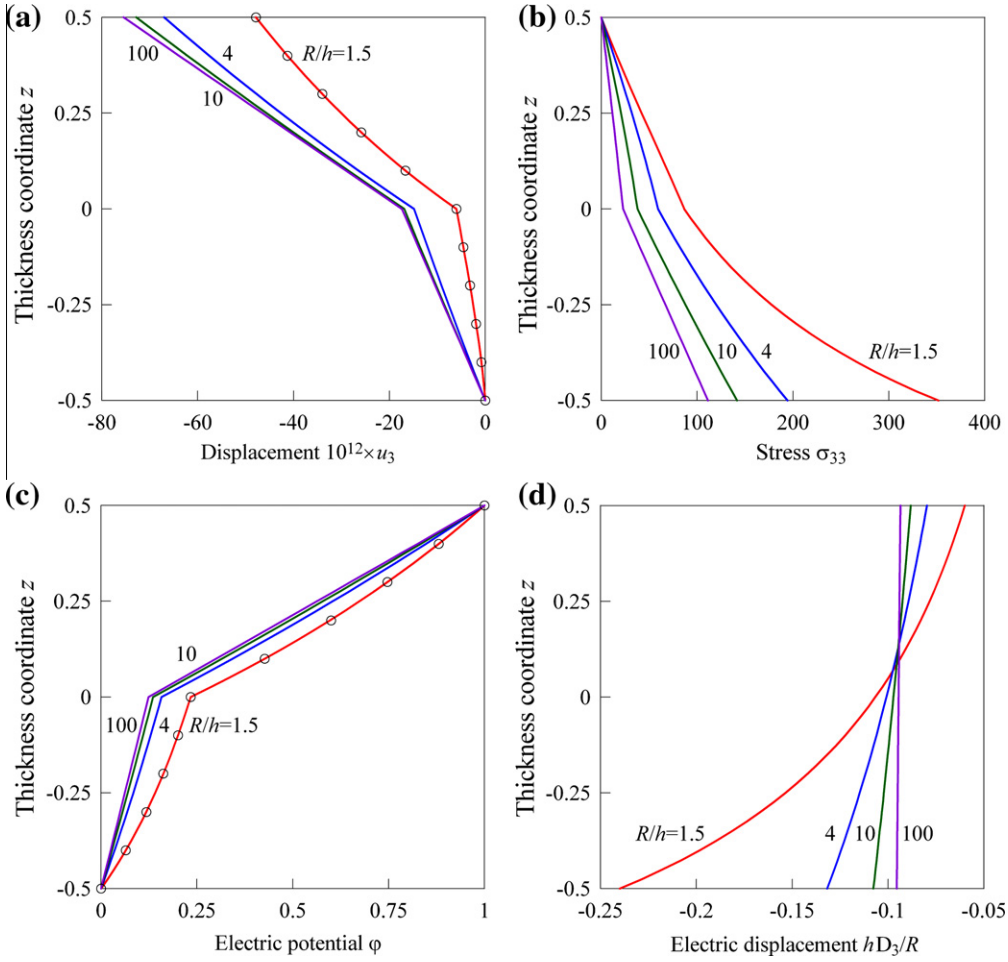

Fig. 9. Distributions of transverse displacement, transverse normal stress, electric potential and electric displacement in the thickness direction of the two-layer spherical shell under electric loading for $I_1 = I_2 = 7$: SaS method (——) and Heyliger and Wu (○).

thicknesses of piezoelectric layers for different values of the slenderness ratio R/h employing seven SaS for each layer. As can be seen, the boundary conditions on bottom and top surfaces and the continuity conditions at layer interfaces for transverse stress and electric displacement components are satisfied with a high accuracy. This statement is confirmed convincingly in Fig. 5 by means of logarithmic errors

$$\delta_\alpha^{\pm} = \lg|\bar{\sigma}_{\alpha 3}(\pm 0.5)|, \quad \delta_3^{-} = \lg|\bar{\sigma}_{33}(-0.5)|,$$
$$\delta_3^{+} = \lg|\bar{\sigma}_{33}(0.5) - p_0|, \quad \delta_4^{-} = \lg|\bar{D}_3(-0.5)|, \tag{55}$$

which characterize the accuracy of fulfilling the boundary conditions for the transverse stresses and electric displacement. It is necessary to note that the proposed SaS method provides a monotonic convergence except for one curve in Fig. 5(a) that is impossible with *equally spaced* SaS (Kulikov and Plotnikova, 2011b). However, the accuracy of computations is slightly worse than in a piezoelectric angle-ply plate formulation (Kulikov and Plotnikova, 2013b).

7.2. Angle-ply shell with attached piezoelectric layers under electric loading

Next, we consider the same angle-ply graphite-epoxy cylindrical shell [45/-45] with attached PZT-4 layers subjected to electric loading. The boundary conditions on the bottom and top surfaces of the shell are

$$\sigma_{13}^{[0]} = \sigma_{13}^{[N]} = \sigma_{23}^{[0]} = \sigma_{23}^{[N]} = \sigma_{33}^{[0]} = \sigma_{33}^{[N]} = 0, \quad D_3^{[0]} = 0, \quad \varphi^{[N]} = \varphi_0 \sin\frac{\pi\theta_1}{L}, \tag{56}$$

where $\varphi_0 = 1$ V.

Tables 8 and 9 also demonstrate the high potential of the developed piezoelectric shell formulation in the case of electric loading. Fig. 6 shows distributions of the transverse stresses and electric potential through the thickness of a shell and the electric displacement through the thicknesses of piezoelectric layers utilizing as usual seven SaS for each layer. It is seen that the boundary conditions on both outer surfaces and continuity conditions at layer interfaces for transverse shear stresses and electric displacement are satisfied correctly. Additionally, we present in Fig. 7 the logarithmic errors defined by Eq. (55) with $p_0 = 0$, which help to assess the accuracy of fulfilling the boundary conditions for transverse stresses and electric displacement on outer surfaces.

8. 3D exact solution for piezoelectric laminated spherical shells

Finally, we study a symmetric deformation of the piezoelectric laminated spherical shell subjected to mechanical and electric loads acting on its bottom and top surfaces considering the most general boundary conditions

$$u_3^{[0]} = u_0^{-} \quad \text{or} \quad \sigma_{33}^{[0]} = p_0^{-}, \quad u_3^{[N]} = u_0^{+} \quad \text{or} \quad \sigma_{33}^{[N]} = p_0^{+}, \tag{57}$$

Table 11
Results for a two-layer spherical shell with $R/h = 1.5$ under electric loading.

I_n	$10^{12} \times u_3$ (0)	$10^{12} \times u_3(0.5)$	φ (0)	$\sigma_{11}(-0.5)$	$\sigma_{11}(0.5)$	$\sigma_{33}(-0.5)$	$\sigma_{33}(0.5)$	$10^2 \times D_3(-0.5)$	$10^2 \times D_3(0.5)$
3	−6.0427	−47.868	0.23335	−137.54	−115.63	314.68	2.4411	−33.346	−8.5933
5	−6.0240	−47.863	0.23356	−142.08	−117.55	350.39	0.6378	−35.935	−8.9944
7	−6.0241	−47.862	0.23356	−141.88	−117.65	351.81	−0.0670	−35.997	−8.9994
9	−6.0241	−47.862	0.23356	−141.90	−117.64	351.79	−0.0082	−35.998	−8.9995
11	−6.0241	−47.862	0.23356	−141.90	−117.64	351.79	−0.0021	−35.998	−8.9995
13	−6.0241	−47.862	0.23356	−141.90	−117.64	351.79	−0.0008	−35.998	−8.9995
Exact	−6.03	−47.86	0.234						

$$\varphi^{[0]} = \varphi_0^- \quad \text{or } D_3^{[0]} = q_0^-, \quad \varphi^{[N]} = \varphi_0^+ \quad \text{or } D_3^{[N]} = q_0^+. \tag{58}$$

Due to spherical symmetry, we search a solution of the problem as follows:

$$u_1^{(n)i_n} = 0, \quad u_2^{(n)i_n} = 0, \quad u_3^{(n)i_n} = u_{30}^{(n)i_n}, \quad \varphi^{(n)i_n} = \varphi_0^{(n)i_n}. \tag{59}$$

The use of Eq. (59) in Eqs. (17), (18), (21), (25), (26), (30), (31), (32), (33), (39), and (40) yields a system of linear algebraic equations

$$\frac{\partial \Pi}{\partial u_{30}^{(n)i_n}} = 0, \quad \frac{\partial \Pi}{\partial \varphi_0^{(n)i_n}} = 0. \tag{60}$$

The linear system (60) is solved by a method of Gaussian elimination.

As accepted throughout this paper, the described algorithm was performed with the Symbolic Math Toolbox of MATLAB to address the symbolic computations.

8.1. Piezoelectric two-layer spherical shell under mechanical loading

Consider a spherical shell composed of PZT-5 and (Pb, Ca)($Co_{1/2}W_{1/2}$) TiO_3 layers with equal thicknesses (Heyliger and Wu, 1999). The electromechanical properties of both materials are given in Table 1. The boundary conditions on the bottom and top surfaces are taken as follows:

$$u_3^{[0]} = 0, \quad \varphi^{[0]} = 0, \quad \sigma_{33}^{[N]} = p_0, \quad \varphi^{[N]} = 0, \tag{61}$$

where $p_0 = 1$ Pa .

Table 10 shows that the proposed formulation based on the SaS method can be applied efficiently to 3D exact solutions of electroelasticity for very thick piezoelectric laminated spherical shells. Fig. 8 displays the distributions of the transverse displacement and transverse normal stress, electric potential and electric displacement through the thickness of a shell for different values of the slenderness ratio R/h by using seven SaS for each layer, where R is the radius of the middle surface. It is seen that the boundary conditions on the bottom and top surfaces and the continuity conditions at the layer interface are satisfied with a high accuracy.

8.2. Piezoelectric two-layer spherical shell under electric loading

In this section, we study a similar piezoelectric two-layer spherical shell subjected to electric loading and consider the following boundary conditions (Heyliger and Wu, 1999):

$$u_3^{[0]} = 0, \quad \varphi^{[0]} = 0, \quad \sigma_{33}^{[N]} = 0, \quad \varphi^{[N]} = \varphi_0, \tag{62}$$

where $\varphi_0 = 1$ V.

Table 11 lists the results of the convergence study through the use of a various number of SaS for very thick spherical shells. Fig. 9 presents the distributions of transverse displacement and transverse normal stress, electric potential and electric displacement through the thickness of the shell for different slenderness ratios R/h employing again seven SaS for each layer. As can be seen, boundary conditions on the bottom and top surfaces and continuity conditions at the layer interface are fulfilled properly.

9. Conclusions

An efficient approach to 3D exact solutions of electroelasticity for piezoelectric laminated shells has been proposed. It is based on the new method of SaS located at Chebyshev polynomial nodes inside each layer and interfaces as well. The stress analysis is based on the 3D constitutive equations of piezoelectricity and gives an opportunity to obtain the 3D exact solutions for thick and thin piezoelectric cross-ply and angle-ply shells with a specified accuracy.

Acknowledgments

This work was supported by Russian Ministry of Education and Science under Grant No 1.472.2011.

References

Burden, R.L., Faires, J.D., 2010. Numerical Analysis, ninth ed. Brooks/Cole, Cengage Learning, Boston.
Carrera, E., 2002. Theories and finite elements for multilayered, anisotropic, composite plates and shells. Archives of Computational Methods in Engineering 9, 1–60.
Carrera, E., 2003. Theories and finite elements for multilayered plates and shells: a unified compact formulation with numerical assessment and benchmarking. Archives of Computational Methods in Engineering 10, 215–296.
Carrera, E., Brischetto, S., Nali, P., 2011. Plates and Shells for Smart Structures: Classical and Advanced Theories for Modeling and Analysis. John Wiley & Sons Ltd.
Chen, C.Q., Shen, Y.P., 1996. Piezothermoelasticity analysis for a circular cylindrical shell under the state of axisymmetric deformation. International Journal of Engineering Science 34, 1585–1600.
Chen, C.Q., Shen, Y.P., Wang, X.M., 1996. Exact solution of orthotropic cylindrical shell with piezoelectric layers under cylindrical bending. International Journal of Solids and Structures 33, 4481–4494.
Chen, W.Q., Ding, H.J., Xu, R.Q., 2001. Three-dimensional static analysis of multilayered piezoelectric hollow spheres via the state space method. International Journal of Solids and Structures 38, 4921–4936.
Cheng, Z.Q., Reddy, J.N., 2002. Asymptotic theory for laminated piezoelectric circular cylindrical shells. AIAA Journal 40, 553–558.
Dube, G.P., Kapuria, S., Dumir, P.C., 1996. Exact piezothermoelastic solution of simply-supported orthotropic circular cylindrical panel in cylindrical bending. Archive of Applied Mechanics 66, 537–554.
Dumir, P.C., Dube, G.P., Kapuria, S., 1997. Exact piezoelastic solution of simply-supported orthotropic circular cylindrical panel in cylindrical bending. International Journal of Solids and Structures 34, 685–702.
Heyliger, P., 1997. A note on the static behavior of simply-supported laminated piezoelectric cylinders. International Journal of Solids and Structures 34, 3781–3794.
Heyliger, P., Wu, Y.C., 1999. Electroelastic fields in layered piezoelectric spheres. International Journal of Engineering Science 37, 143–161.
Kapuria, S., Dumir, P.C., Sengupta, S., 1997a. An exact axisymmetric solution for a simply supported piezoelectric cylindrical shell. Archive of Applied Mechanics 67, 260–273.
Kapuria, S., Dumir, P.C., Sengupta, S., 1997b. Nonaxisymmetric exact piezothermoelastic solution for laminated cylindrical shell. AIAA Journal 35, 1792–1795.
Kapuria, S., Sengupta, S., Dumir, P.C., 1997c. Three-dimensional solution for simply-supported piezoelectric cylindrical shell for axisymmetric load. Computer Methods in Applied Mechanics and Engineering 140, 139–155.
Kapuria, S., Sengupta, S., Dumir, P.C., 1997d. Three-dimensional solution for a hybrid cylindrical shell under axisymmetric thermoelectric load. Archive of Applied Mechanics 67, 320–330.

Kulikov, G.M., Plotnikova, S.V., 2008. Geometrically exact four-node piezoelectric solid-shell element. Mechanics of Advanced Materials and Structures 15, 199–207.

Kulikov, G.M., Plotnikova, S.V., 2011a. Finite rotation piezoelectric exact geometry solid-shell element with nine degrees of freedom per node. Computers, Materials & Continua 23, 233–264.

Kulikov, G.M., Plotnikova, S.V., 2011b. Solution of statics problems for a three-dimensional elastic shell. Doklady Physics 56, 448–451.

Kulikov, G.M., Plotnikova, S.V., 2012a. Exact 3D stress analysis of laminated composite plates by sampling surfaces method. Composite Structures 94, 3654–3663.

Kulikov, G.M., Plotnikova, S.V., 2012b. On the use of sampling surfaces method for solution of 3D elasticity problems for thick shells. ZAMM – Journal of Applied Mathematics and Mechanics 92, 910–920.

Kulikov, G.M., Plotnikova, S.V., 2013a. Advanced formulation for laminated composite shells: 3D stress analysis and rigid-body motions. Composite Structures 95, 236–246.

Kulikov, G.M., Plotnikova, S.V., 2013b. Three-dimensional exact analysis of piezoelectric laminated plates via sampling surfaces method. International Journal of Solids and Structures 50, http://dx.doi.org/10.1016/j.ijsolstr.2013.02.015.

Pagano, N.J., 1969. Exact solutions for composite laminates in cylindrical bending. Journal of Composite Materials 3, 398–411.

Pagano, N.J., 1970. Exact solutions for rectangular bidirectional composites and sandwich plates. Journal of Composite Materials 4, 20–34.

Soldatos, K.P., Hadjigeorgiou, V.P., 1990. Three-dimensional solution of the free vibration problem of homogeneous isotropic cylindrical shells and panels. Journal of Sound and Vibration 137, 369–384.

Tauchert, T.R., Ashida, F., Noda, N., Adali, S., Verijenko, V., 2000. Developments in thermopiezoelasticity with relevance to smart composite structures. Composite Structures 48, 31–38.

Tzou, H.S., 1993. Piezoelectric Shells: Distributed Sensing and Control of Continua. Kluwer-Academic, Dordrecht.

Vlasov, B.F., 1957. On the bending of a rectangular thick plate. Trans Moscow State University 2, 25–31.

Wang, X., Zhong, Z., 2003. Three-dimensional solution of smart laminated anisotropic circular cylindrical shells with imperfect bonding. International Journal of Solids and Structures 40, 5901–5921.

Wu, C.P., Lo, J.Y., Chao, J.K., 2005. A three-dimensional asymptotic theory of laminated piezoelectric shells. Computers, Materials & Continua 2, 119–137.

Wu, C.P., Liu, K.Y., 2007. A state space approach for the analysis of doubly curved functionally graded elastic and piezoelectric shells. Computers, Materials & Continua 6, 177–199.

Wu, C.P., Syu, Y.S., 2007. Exact solutions of functionally graded piezoelectric shells under cylindrical bending. International Journal of Solids and Structures 44, 6450–6472.

Wu, C.P., Syu, Y.S., Lo, J.Y., 2007. Three-dimensional solutions for multilayered piezoelectric hollow cylinders by an asymptotic approach. International Journal of Mechanical Sciences 49, 669–689.

Wu, C.P., Chiu, K.H., Wang, Y.M., 2008. A review on the three-dimensional analytical approaches of multilayered and functionally graded piezoelectric plates and shells. Computers, Materials & Continua 8, 93–132.

Wu, C.P., Huang, S.E., 2009. Three-dimensional solutions of functionally graded piezo-thermo-elastic shells and plates using a modified Pagano method. Computers, Materials & Continua 12, 251–281.

Wu, C.P., Tsai, T.C., 2012. Exact solutions of functionally graded piezoelectric material sandwich cylinders by a modified Pagano method. Applied Mathematical Modelling 36, 1910–1930.

Xu, K., Noor, A.K., 1996. Three-dimensional analytical solutions for coupled thermo-electroelastic response of multilayered cylindrical shells. AIAA Journal 34, 802–810.